Title

Stimulating Antitumoral Immunity by Percutaneous Cryoablation and Combination Immunoadjuvant Therapy in a Murine Model of Hepatocellular Carcinoma

Journal

Journal of Vascular and Interventional Radiology, 34(9)

ISSN

1051-0443

Authors

Mandt, Tyler

Bangar, Amandip

Sauceda, Consuelo

et al.

Publication Date

2023-09-01

DOI

10.1016/j.jvir.2023.05.008

Peer reviewed

Published in final edited form as:
J Vasc Interv Radiol. 2023 September ; 34(9): 1516–1527.e6. doi:10.1016/j.jvir.2023.05.008.

Stimulating Antitumoral Immunity by Percutaneous Cryoablation and Combination Immunoadjuvant Therapy in a Murine Model of Hepatocellular Carcinoma

Tyler Mandt, MD,
Amandip Bangar, BS,
Consuelo Sauceda, BS,
Manasi Das, PhD,
Carolyn Moderbacher, PhD,
Mansur Ghani, MD,
Nicholas Webster, PhD,
Isabel Newton, MD, PhD

Health Department of Radiology (T.M., A.B., C.S., M.D., M.G.) and San Diego Veteran's Affairs (N.W., I.N.), University of California San Diego, San Diego, and La Jolla Institute for Allergy and Immunology (C.M.), La Jolla, California

Abstract

Purpose: To test the hypothesis that antitumoral immunity can be induced after cryoablation (cryo) of hepatocellular carcinoma (HCC) through coadministration of the immunostimulant CpG and an immune checkpoint (programmed cell death 1 [PD-1]) inhibitor.

Materials and Methods: Sixty-three immunocompetent C57BL/6J mice were generated with 2 orthotopic HCC tumor foci: 1 for treatment and 1 to observe for antitumoral immunity. Tumors were treated with incomplete cryo alone or intratumoral CpG and/or a PD-1 inhibitor. The primary endpoint was death or when the following criteria for sacrifice were met: tumor > 1 cm (determined using ultrasound) or moribund state. Antitumoral immunity was assessed using flow cytometry and histology (tumor and liver) as well as enzyme-linked immunosorbent assay (serum). Analysis of variance was used for statistical comparisons.

Results: At 1 week, the nonablated satellite tumor growth was reduced by 1.9-fold ($P = .047$) in the cryo + CpG group and by 2.8-fold ($P = .007$) in the cryo + CpG + PD-1 group compared with that in the cryo group. Compared with cryo alone, the time to tumor progression to endpoints was also prolonged for cryo + CpG + PD-1 and cryo + CpG mice, with log-rank hazard ratios of 0.42 ($P = .031$) and 0.27 ($P < .001$), respectively. Flow cytometry and histology showed increased cytotoxic T-cell infiltration ($P = .002$) and serum levels of the proinflammatory cytokine interferon-γ ($P = .015$) in tumors and serum of cryo + CpG mice compared with those in tumors

Address correspondence to I.N., Department of Radiology, University of California San Diego, 3350 La Jolla Village Dr, San Diego, CA 92161; inewton@health.ucsd.edu; Twitter handle: @theIIMD.

Figures E1–E3, Tables E1–E4, and Appendix A can be found by accessing the online version of this article on www.jvir.org and selecting the Supplemental Material tab.

and serum of mice treated with cryo alone. High serum levels of the anti-inflammatory cytokine tumor growth factor-β and the proangiogenesis chemokine C-X-C motif chemokine ligand 1 were correlated with a shorter time to endpoints and faster tumor growth.

Conclusions: Cryo combined with the immunostimulant CpG promoted cytotoxic T-cell infiltration into tumors, slowed tumor growth, and prolonged the time to progression to endpoints in an aggressive murine HCC model.

The incidence of hepatocellular carcinoma (HCC) and its resulting mortality are rising (1). Most patients are ineligible for curative resection or liver transplantation. Thermal ablation can offer a cure; however, recurrence after incomplete ablation can lead to greater proliferation and resistance to treatment (2–4). HCC evades the immune system by expressing the immune checkpoint protein programmed death ligand 1 and recruiting immunosuppressive M2 macrophages, mature daughter cells of myeloid-derived suppressor cells (5). Tumor cells can avoid immune detection by inactivating T cells. T-cell anergy occurs when programmed death ligand 1 on tumor cells binds to programmed cell death 1 (PD-1) on T cells. PD-1 inhibitors can reverse this T-cell tolerance; however, they produce a clinical response in only 27%–33% of patients with HCC (6).

Thermal ablation alone can rarely induce the “abscopal effect,” a systemic antitumoral immune response culminating in regression of distant metastatic disease (7). Among all forms of thermal ablation, cryoablation (cryo) is thought to induce the most potent tumor-specific inflammatory response, causing increased levels of inflammatory mediators (interleukin [IL]-1, IL-6, nuclear factor-κB, and tumor necrosis factor-α) and increased tumor antigen loading into dendritic cells (DCs) (8). Tumor antigen uptake by plasmacytoid dendritic cells (pDCs) is thought to link the innate and adaptive antitumoral immune responses, which is important for the abscopal effect. pDCs are a subset of DCs enriched in blood and peripheral lymphoid tissue, including in the liver (9). Immunostimulants, such as unmethylated cytosine-phosphate-guanine oligodeoxynucleotides (CpGs), can promote recognition and presentation of tumor antigens, which may help overcome the immunosuppressive microenvironment of the liver. CpGs are a class of toll-like-receptor (TLR) 9 agonists that induce pDC antigen presentation and proinflammatory cytokine production (10,11). Early clinical trials of CpG established an excellent safety profile but underwhelming clinical outcomes compared with those in animal studies (12). Induction of a durable response may depend on the availability of tumor antigens at the time of CpG-induced pDC activation (13). There may also be a role of coadministration of CpG with immune checkpoint inhibitors in HCC because this combination had a synergistic effect against metastatic melanoma (10,14). However, there are no studies evaluating the combination of thermal ablation with an immunostimulant (CpG or other TLR agonist) and a checkpoint inhibitor for HCC (15). Using an aggressive murine model of HCC, this study tested the hypothesis that cryo plus CpG and a PD-1 inhibitor can induce antitumoral immunity.

MATERIALS AND METHODS

The Institutional Animal Care and Use Committee approved all procedures (protocol S06319).

Study Design and Intrahepatic HCC Implantation

This study included 63 male wild-type C57BL/6J mice (Jackson Laboratories, Bar Habor, Maine), based on a power analysis performed using G*Power 3.1 (Heinrich Heine University Dusseldorf), with an effect size of 0.80 derived from pilot data, error probability of 0.05, and power of 0.85, yielding a calculated total sample size of 7 per group plus 3 mice to account for anticipated death due to disease progression and another 3 mice for histologic/flow cytometric analysis for a sample size of 13 per group. The nointervention observation arm included 11 mice because there was no need to account for procedural mortality. The mice were transitioned from an ad libitum normal chow diet to a nonalcoholic steatohepatitis (NASH)–inducing diet (D12079, Western Diet; Research Diets, New Brunswick, New Jersey) at 6 weeks of age, at least 4 weeks before injection of RIL-175 cells, an HCC cell line established in C57BL/6 mice via transfer of $HRas^{V12}$-transduced$p53^{-/-}$ fetal hepatoblasts (16). Further details can be found in Appendix A (available online on the article's Supplemental Material page at www.jvir.org.). Male mice were studied due to better engraftment rates than those of females, possibly due to greater immunotolerance because the RIL-175 cell line originated in a male mouse. Livers with NASH demonstrated better engraftment rates than normal livers (data not shown).

A 70-MHz ultrasound (US) transducer (Vevo MD Ultra High Frequency US System; VisualSonics, Fujifilm, Ontario, Canada) was used to guide RIL-175 cell injections into the right and left lateral hepatic lobes: 1 for observation as a "satellite" lesion and the other for treatment. A 22-gauge needle preloaded with RIL-175 cells suspended in extracellular matrix (detailed in Appendix A, available online at www.jvir.org) was advanced through a 19-gauge introducer needle (CT2011 Temno Merit Medical, South Jordan, Utah) to limit tract seeding. The animals were monitored during the periprocedural period. The Animal Research: Reporting of In Vivo Experiments (ARRIVE) guidelines and Figure 1 contain additional details of study design, including subject experimental group allocation and exclusion.

Tumor Volume Characterization and Endpoints

Tumors were imaged using US at least weekly by an assessor (T.C.M.) who was blinded to the intervention. A research team, consisting of an interventional radiology resident and 2 research scientists, was trained and overseen by an attending interventional radiologist scientist (I.G.N.). Tumors were measured along their greatest dimensions in the axial and sagittal planes, and only viable tumors were measured. Tumor volumes were calculated using the following equation: $Volume = \frac{\pi}{6}(x * y * z)$, where x is the left-to-right diameter, y is the craniocaudal diameter, and z is the anteroposterior diameter. The threshold tumor size was ≥5 mm for treatment. At the time of ablation, there were no statistical differences in tumor size among the groups (Tables E1 and E2) available online at www.jvir.org).

To normalize heterogeneity in tumor volumes at the start of treatment, fold changes in tumor volumes were calculated at 1 week after treatment compared with volumes at the time of treatment. Descriptive statistics are featured in Table E3 (available online at www.jvir.org). The sacrifice criteria for mice included in the time-to-endpoint analysis were tumors >1 cm in any dimension or difficulty with ambulating, poor grooming, weight loss, or external

signs of injury. Due to rapid tumor growth, 3 observation, 3 cryo-alone, and 4 cryo + PD-1 mice met the >1-cm sacrifice criterion at 1 week after treatment, so tissues were collected for flow cytometry/histology. For comparison, 3 mice from the cryo + PD-1 and 3 mice from the cryo + PD-1 + CpG groups were also sacrificed at 1 week after treatment for flow cytometry/histology. Two mice from each of these groups did not meet the sacrifice criteria and were, thus, excluded from the time-to-endpoint analysis. As depicted in Figure 1 and described in the ARRIVE guidelines, 1 subject from the cryo and 1 subject from the cryo + CpG groups were excluded from the time-to-endpoint and tumor growth analyses because of 1 or both tumor volumes exceeding the total mean tumor volume by 2 standard deviations across all treatment arms, a predetermined criterion for outlier exclusion. One mouse each from the cryo + PD-1, cryo + CpG, and cryo + CpG + PD-1 groups did not have a satellite tumor for the tumor growth analysis 7 days after the procedure. Normal liver tissue, spleen tissue, ablated tumor tissue, and nonablated tumor tissue were harvested, and portions of these tissues were submitted for flow cytometry and histology/immunohistochemistry.

US-Guided Percutaneous cryo and US-Guided CpG and PD-1 Inhibitor Injection

One week after tumor injections, on the day of ablation, the mice were randomized into the following experimental groups using the “randbetween” function in Excel (Microsoft, Redmond, Washington): cryo alone, Cryo + PD-1, cryo + CpG, cryo + CpG + PD-1, and observation. Randomization occurred prior to the preprocedural measurements; therefore, mice in some groups did not have tumor engraftment and were, thus, excluded from the analysis (further detailed in the ARRIVE guidelines and Fig 1). A custom-made 17-gauge, 3-cm cryo probe (Galil IceSeed; Boston Scientific, Marlborough, Massachusetts) was used for cryos with 3 cycles of 1-minute freezes at 50% power (Fig E1, available online at www.jvir.org). Approximately 75% of the tumor was targeted for ablation to simulate incomplete ablation.

CpG and/or a PD-1 inhibitor were administered percutaneously under US guidance immediately after ablation. One exception was a cohort of mice that received CpG 3 days prior to and at the time of cryo (3 mice receiving cryo + CpG and 3 mice receiving cryo + CpG + PD-1) to potentially prime the immune system. Data from these mice contributed to the time-to-endpoint analysis, tumor growth analysis, and serum cytokine analyses but not the flow cytometry or histology data. For CpG treatment, 100 μg of CpG ODN 2395, a type C CpG (IAX-200-007-M001; Adipogen, San Diego, California), diluted in endotoxin-free saline, was injected in 3 fractions along the tumor ablation margins. For PD-1 inhibitor treatment, 10 mg/kg of anti-PD-1 antibody (BE0146, InVivoMAb anti-mouse PD-1; Bio X Cell, Deer Park, Illinois) was injected percutaneously into the spleen or portal vein to maximize hepatic uptake. Animals from a single cage were normally subjected to a randomized intervention before moving onto the next cage.

Flow Cytometry

Flow cytometry of lymphocytes from ablated and non-ablated tumors was performed at 1 week after treatment.

Enzyme-Linked Immunosorbent Assay

Baseline tail vein blood (25 μL) was drawn prior to tumor injection. After treatment, blood was drawn at 24, 48, and 72 hours and then weekly until the endpoint was reached. Blood processing is detailed in Appendix A (available online at www.jvir.org).

Histology

Tissue samples were sliced at 1-mm thickness prior to fixation. The technical details regarding tissue processing are shown in Appendix A (available online at www.jvir.org). Slides were scanned, and positive pixels were quantitated using the ImageScope software package (Leica 2021, Deer Park, Illinois) and divided by the total quantitated area to determine the relative pixel positivity. Only viable tissue was quantitated. For each mouse, 1 slide containing 1–2 slices of ablated tumor and 1–2 slices of nonablated tumor (the slice number depended on the amount of tissue) were analyzed. Because no statistically significant differences were demonstrated, the ablated and nonablated tumor tissue data were pooled to maximize the amount of viable tissue analyzed.

Data Analysis and Statistical Methods

Flow cytometry data were analyzed using FlowJo (FlowJo, Ashland, Oregon) and imported into Prism 9 (GraphPad, San Diego, California). Prism was used for plot generation, and 1-way analysis of variance, Fisher least significant difference test, and log-rank hazard ratio were used for Kaplan-Meier curves. A P value of <.05 defined statistical significance. A 2-tailed t-test was used for correlation matrixes. Correlations with P <.05 were plotted. Data analysis was not blinded.

RESULTS

HCC Foci Grew in the Mouse NASH Livers and Were Safely Treated with Percutaneous Cryo

Untreated, engrafted RIL-175 cell tumors reached 1 cm by 2 weeks after implantation. The tumors appeared spheroidal and hypoechoic on US relative to hepatic parenchyma (Fig 2). Sixty-four percent of tumors in the observation group and 55% and 57% of tumors in the cryo and cryo + PD-1 groups, respectively, were >1 cm in any dimension 2 weeks after treatment (or 3 weeks after injection) (Table E4, available online at www.jvir.org). One had just 1 tumor engraft.

Treatment with Cryo + CpG + PD-1 or Cryo + CpG Retarded Tumor Growth

Treatment with CpG at the time of cryo slowed the growth of both ablated and nonablated satellite tumors. The nonablated satellite tumor growth was reduced by 1.9-fold (P = .0472) in the cryo + CpG group and by 2.8-fold (P = .007) in the cryo + CpG + PD-1 group compared with that in the cryo group (Fig 3a). The addition of the PD-1 inhibitor did not change tumor growth compared with cryo alone in satellite or ablated tumors. The satellite tumor growth rate varied the most in the cryo and cryo + PD-1 groups and least in the cryo + CpG + PD-1 group (Table E5, available online at www.jvir.org). The ablated tumor growth

rate decreased in the cryo + CpG group compared with that in cryo ($P = .045$) and cryo + PD-1 ($P = .029$) groups (Fig 3b).

Prolonged Time to Endpoints in Mice Treated with CpG

Animals treated with CpG, regardless of PD-1, had a longer time to endpoints than mice receiving no treatment, cryo alone, or cryo + PD-1. Figure 2c shows the duration until euthanasia after treatment. Compared with cryo alone, CpG treatment was associated with a significantly prolonged time to endpoints independent of the PD-1 inhibitor, with log-rank hazard ratios of 0.42 ($P = .031$) and 0.27 ($P < .001$) for the cryo + CpG and cryo + CpG + PD-1 groups, respectively. At 18 days after treatment, 12 of 16 (75%) mice in the CpG-treated groups lived beyond 2 weeks after treatment, whereas 3 of 30 (10%) mice in the remaining groups had not yet met the sacrifice criteria. One mouse treated with cryo + CpG + PD-1 survived over 100 days after treatment and had no detectable tumor by US.

Antitumoral Immune Cells Increased in Tumors of Mice Treated with Cryo + CpG

Histology and flow cytometry showed increased antitumoral immune cells in tumors from mice treated with cryo + CpG. Using hematoxylin and eosin staining, the tumor tissue was found to be composed of small cells with large nuclear-to-cytoplasmic ratios, disorganized architecture with interspersed fibrosis, and lobulated morphology (Fig 4a). Ablated tissue was necrotic and acellular. Large satellite tumors showed a rim of viable tumor cells with central necrosis (Fig 4b). Cytotoxic T cells, which are positive for CD8, accumulated at the tumor periphery of cryo + CpG + PD-1 ablated tumors, suggesting infiltration of these antitumor T cells from adjacent liver. FOXP3 is a lymphocyte marker specific to an immunosuppressive subtype of T cells, T-regulatory (Treg) cells (17). Cytotoxic CD8+ T cells and immunosuppressive FOXP3+ cells from pooled satellite and ablated tumors (nonnecrotic regions) and the liver were quantitated from each treatment group (Fig 4c). CD8+ staining was significantly increased in pooled ablated and nonablated tumor samples from cryo + CpG mice compared with that in samples from observation ($P = .028$) and cryo + PD-1 ($P = .046$) mice but not significantly increased compared with that in samples from cryo only ($P = .121$) and cryo + CpG + PD-1 ($P = .118$) mice. An apparent increase in FOXP3+ staining in the cryo group compared with that in the observation group did not meet statistical significance ($P = .092$).

Flow cytometry showed cytotoxic CD8+ T-cell enrichment in ablated cryo + CpG ($P = .002$) and cryo + CpG + PD-1 ($P = .046$) tumors compared with that in cryo-alone tumors (Fig 5). PD-1 inhibition did not affect ablated or satellite intratumoral cytotoxic CD8+ T-cell concentrations. Although not statistically significant, activated natural killer cells (CD137+NK1.1+) trended higher in ablated and nonablated tumors of subjects treated with cryo + CpG and cryo + CpG + PD-1 than in tumors of the observation group and cryo-alone controls. Cytotoxic T cells expressing markers of antigen exposure (CD8+ CD44+) (18) demonstrated increased PD-1 expression (CD8+ CD44+ PD+) in ablated tumors of the CpG-treated groups compared with that in the cryo ($P = .005$) and cryo + PD-1 ($P < .001$) groups in both ablated and satellite tumors. Figure E2 (available online at www.jvir.org) shows the results of additional lymphocyte markers that were tested.

Proinflammatory Cytokines Increased after Cryo + CpG Cotreatment

Injection of CpG around the ablation zone at the time of cryo was associated with increased serum levels of proinflammatory cytokines and mixed changes in anti-inflammatory cytokines. The serum levels of proinflammatory (interferon-γ [IFN-γ]) and anti-inflammatory cytokines (IL-10 and transforming growth factor-β1 [TGF-β1]) were quantitated using enzyme-linked immunosorbent assay at multiple time points (Fig 6a). Additional cytokines were tested and are presented in Figure E3 (available online at www.jvir.org). The level of the proinflammatory cytokine IFN-γ was elevated in the CpG-treated groups, peaking at 48 hours and tapering to baseline by 2 weeks. The level of the anti-inflammatory cytokine IL-10 was elevated in the CpG-treated groups, peaking at 24 hours and tapering at 1 week. The level of the anti-inflammatory cytokine TGF-β1 was elevated in the cryo + CpG + PD-1 group, peaking at 24–48 hours and tapering by 1–2 weeks.

A linear (Pearson) correlation was modeled on serum cytokine data against time to endpoints as well as ablated and satellite tumor growth rates (Fig 6b). Statistically significant results were demonstrated, with only ablated tumor growth changes reaching statistical significance. C-X-C motif chemokine ligand 1 (CXCL1) is a proangiogenic chemokine that recruits immunosuppressive cells to tumors (19). High serum CXCL1 levels at 1 week after treatment were associated with a shorter time to endpoints ($P = .017$). The CpG-treated groups clustered at low CXCL1 levels and a longer time to endpoints. In contrast, both the cryo + PD-1 and observation groups had a shortened time to endpoints, clustering into high and moderate CXCL1 concentrations, respectively. Increased levels of immunosuppressive IL-10 at 1 week after treatment were associated with improved time to endpoints ($P = .028$). The CpG-treated groups had a longer time to endpoints and higher IL-10 concentrations, possibly reflecting a negative feedback mechanism. High serum levels of immunosuppressive TGF-β3 at 72 hours after treatment were associated with a shortened time to endpoints ($P = .033$). Cryo + CpG + PD-1 mice grouped at low TGF-β3 concentrations and a prolonged time to endpoints. At 48 hours, increased levels of the immunostimulatory cytokines IL-1β ($P = .031$) and tumor necrosis factor-α ($P = .028$) were correlated with decreased ablated tumor growth. At 1 week after treatment, increased concentrations of immunosuppressive TGF-β2 were correlated with increased ablated tumor growth ($P = .001$). The cryo + CpG + PD-1 group clustered at low TGF-β2 concentrations and decreased ablated tumor growth.

DISCUSSION

This combination of cryo and immunotherapy inhibited disease progression in an aggressive model of HCC in the setting of NASH compared with cryo alone. It slowed tumor growth in not only treated tumors but also untreated satellite tumors. In contrast, cryo alone accelerated tumor growth in a subset of mice, possibly reflecting thermal stress–mediated stimulation of HCC proliferation, as observed in vitro (20). These findings have clinical implications for patients with HCC at all stages because few patients with HCC are eligible for curative therapy and metastatic HCC carries a grim prognosis (4,6).

Tumor growth inhibition in the immunotherapy groups was immune mediated. Flow cytometry and histology demonstrated infiltration of cytotoxic T-cells and activated natural killer cells into treated primary and untreated satellite, or “metastatic,” tumors. Also elevated were the levels of IFN-γ, which stimulates antigen presentation and antitumor immune cells, inhibits immunosuppressive M2 macrophages, and counteracts the immunosuppressive cytokines TGF-β and IL-10 (21). In the cryo + CpG + PD-1 group on day 0, elevation of the levels of IFN-γ and IL-12, a stimulator of proinflammatory IFN-γ secretion (22), was observed in the subset of mice that received CpG 3 days before and at the time of cryo (Fig E2, available online at www.jvir.org). Conversely, the subset of cryo + CpG mice that received early CpG did not demonstrate a similar elevation of the levels of these cytokines. CpG-induced inflammation likely accounts for the transient increase in the serum levels of immunosuppressive IL-10 and TGF-β1 (23).

FOXP3 is a lymphocyte marker of Treg cells, which quell antitumoral immunity (17). TGF-β2 and -β3 induce differentiation of naïve T cells to Treg cells and inhibit cytotoxic CD8+ T-cell activation (17,24). Low serum levels of TGF-β family cytokines are associated with survival in advanced HCC (25), which is congruent with this study. CXCL1 is a proangiogenic chemokine that recruits myeloid-derived suppressor cells, which suppress antitumoral immunity (19). These inhibitory cells are countered by the immune response stimulated by PD-1 inhibition and CpG (26,27); as expected, the CXCL1 levels were lower after PD-1 inhibitor and CpG treatment, and tumor progression was delayed. IL-1β stimulates DCs and other antigen-presenting cells and activates natural killer cells and cytotoxic CD8+ T cells (28); IL-1β levels were inversely correlated with tumor growth.

Increased PD-1 expression in activated (CD44+) cytotoxic CD8+ T cells of the CpG-treated groups likely reflects exhaustion from prolonged exposure to tumor antigens shed by rapidly proliferating tumors (29). However, the addition of the PD-1 inhibitor did not elicit any further reduction in tumor growth. A clinical trial meta-analysis by Pfister et al (30) showed decreased efficacy of PD-1 inhibitor treatment in a murine model of NASH-driven HCC. The same study showed intrahepatic accumulation of PD-1–expressing cytotoxic CD8+ T cells, in which PD-1 inhibition increased and CD8+ T-cell depletion decreased the incidence of NASH-driven HCC. Thus, cytotoxic CD8+ T-cell exhaustion could account for the poor efficacy of PD-1 inhibition in the present study.

Except for a 2013 study (15) that evaluated autologous T-cell therapy with cryo, there are no prior HCC studies evaluating immunotherapy with cryo or combining TLR agonists, such as CpG, with any form of thermal ablation. The combination of CpG therapy and PD-1 inhibition has been tested in melanoma, a tumor with greater neoantigenic variation than HCC; even so, the clinical efficacy was limited (12,31). Because tumor antigen uptake by DCs is a vital step in linking the innate and adaptive antitumoral immune responses, induction of an abscopal effect may have been precluded by insufficient tumor antigens at the time of CpG administration. Cryo can solve this predicament. Nierkens et al (13) showed that intratumoral CpG administration at the time of cryo of murine melanoma led to 100% survival following tumor rechallenge but <50% survival if administered 1 day before or after cryo. These findings are congruent with this study, in which coadministration of CpG or CpG + PD-1 with cryo halted HCC tumor growth and prolonged survival. The proposed

mechanism by which this combination inhibits tumor growth is through cryo-induced release of abundant tumor antigens with concomitant CpG-mediated pDC stimulation, resulting in increased antigen cross-presentation and circulating proinflammatory IFN-γ, ultimately leading to activated effector lymphocyte infiltration into primary and metastatic tumors (Fig 7).

This study has its limitations. It was designed to test whether combined therapy can improve treatment response after incomplete tumor ablation and not to assess CpG or PD-1 inhibitor as monotherapy. As such, the possibility that CpG alone is sufficient to induce the observed therapeutic effect cannot be excluded but is less likely given the poor efficacy of CpG monotherapy in the literature. Another limitation is the tumor model. Unlike HCC in humans or animal models with spontaneous HCC formation, this orthotopic model involved implantation of tumor cells that should be genetically identical to the recipient mouse. Although tumors engrafted at a high rate, suggesting immunotolerance, and NASH livers were used to recapitulate a clinically relevant tumor microenvironment, it possible that the act of tumor implantation, neoantigen formation through cell line propagation, or small genetic differences between the mice in this study and the tumor cell progenitor mouse could result in a less immunotolerant phenotype compared with that in a spontaneous tumor model, leading to spuriously more effective immunotherapy. Conversely, the high tumor proliferative rate of this tumor model, exceeding that of most human HCCs, may have led to T-cell exhaustion and limited the time window for immune memory formation, potentially compromising the efficacy of the therapy. Another potential limitation was the delivery of the PD-1 inhibitor via an intrasplenic or portal venous approach because PD-1 inhibitors are dosed systemically in clinical practice. The administration method employed in this study maximized the dose to the liver and would, thus, be expected to maximize any potential response to the PD-1 inhibitor. Another limitation of this study is that TLR 9, the receptor for CpG, is expressed in a broader range of immune cells in mice than in humans (primarily B cells and pDCs). Therefore, mice may have a more potent immune response (26).

The results of this preclinical study merit clinical translation. The compounds and techniques have been tested in clinical trials or used in clinical practice and are well tolerated. Initially, the combination of cryo and CpG may be best suited for patients with unresectable or metastatic disease given the induction of a systemic antitumoral response and paucity of therapeutic options for these patients. Given the high rate of HCC recurrence, this approach could also be an adjuvant to curative therapy. Finally, this combination therapy could be effective for malignancies other than HCC, particularly those with high rates of somatic mutation, such as lung, stomach, and colorectal cancers (31).

Supplementary Material

Refer to Web version on PubMed Central for supplementary material.

ACKNOWLEDGMENTS

The study was supported in part by a Resident Research Grant from the RSNA (to T.M.), by grant T32 EB005970 from the National Institutes of Health (to T.M), by grants IBX004848 and IBK005224 from the Department of

Veterans Affairs (to N.J.G.W.), by a Pilot and Feasibility award from the Moores Cancer Center (to I.G.N. and N.J.G.W.).

I.G.N. received support from Boston Scientific/Galil for a cryoablation device and custom cryoprobes, the Society for Interventional Oncology Grant, the UCSD Pedal the Cause Grant, the RSNA Scholar Grant, the Society of Interventional Radiology Foundation Pilot Grant, the Department of Defense grant, and UCSD Academy of Clinician Scholars Grants; received consulting fees from the Boston Scientific Executive Advisory Board, the Varian Advisory Board, AstraZeneca, Genentech, Cur Therapeutics, Replimune, and QED; received speaker fees from Penumbra, the Society for Interventional Radiology, VIVA/VEINS, and UCSD Graduate Course; received support for meetings and travel from the Society for Interventional Oncology, VIVA/VEINS, Penumbra, WAIS, and California Orthopedic Association; is a member of the board of the Society for Interventional Oncology, Western Angiographic and Interventional Society, and The Interventional Initiative; and received equipment from Boston Scientific/Galil. T.M. received grants from the Society of Interventional Oncology, University of California San Diego Moore's Cancer Center, National Institutes of Health, and Radiological Society of North America; received travel support from VIVA/VEINS Conference 2022; and received cryoablation device and custom probes from Boston Scientific/Galil. None of the other authors have identified a conflict of interest.

From the Society of Interventional Oncology Poster Exhibit. February 2, 2022 ("Stimulating antitumoral immunity by percutaneous cryoablation and combination immunoadjuvant therapy in hepatocellular carcinoma").

From the Radiological Society of North America On-Demand Sessions. SSVI07-05. November 29, 2020 ("Stimulating the abscopal effect in hepatocellular carcinoma with cryoablation and immunoadjuvants").

From the Society of Interventional Oncology Poster Exhibit. February 2, 2020 ("Percutaneous Cryoablation and Combination Immunoadjuvant Therapy in a Mouse Model of Hepatocellular Carcinoma").

From the Society of Interventional Oncology Supported Research Plenary. June 9, 2019 ("Combining HCC cryoablation with immunoadjuvants to stimulate the abscopal effect").

ABBREVIATIONS

CXCL1	C-X-C motif chemokine ligand 1
cryo	cryoablation
DC	dendritic cell
IFN-γ	interferon-γ
HCC	hepatocellular carcinoma
IL	interleukin
NASH	nonalcoholic steatohepatitis
pDC	plasmacytoid dendritic cell
PD-1	programmed cell death 1
TGF-β1	transforming growth factor-β1
TLR	toll-like-receptor
US	ultrasound

REFERENCES

1. U.S. Cancer Statistics Working Group. United States cancer statistics. Available at: www.cdc.gov/uscs. Accessed May 13, 2018.

2. Lam VW, Ng KK, Chok KS, et al. Incomplete ablation after radiofrequency ablation of hepatocellular carcinoma: analysis of risk factors and prognostic factors. Ann Surg Oncol 2008; 15:782–790. [PubMed: 18095030]

3. Kong J, Kong L, Ke S, et al. After insufficient radiofrequency ablation, tumor-associated endothelial cells exhibit enhanced angiogenesis and promote invasiveness of residual hepatocellular carcinoma. J Transl Med 2012; 10:1–11. [PubMed: 22214470]

4. Wang JH, Wang CC, Hung CH, Chen CL, Lu SN. Survival comparison between surgical resection and radiofrequency ablation for patients in BCLC very early/early stage hepatocellular carcinoma. J Hepatol 2012; 56:412–418. [PubMed: 21756858]

5. Sultan M, Coyle KM, Vidovic D, Thomas ML, Gujar S, Marcato P. Hide- and-seek: the interplay between cancer stem cells and the immune system. Carcinogenesis 2017; 38:107–118. [PubMed: 27866156]

6. Finn RS, Qin S, Ikeda M, et al. Atezolizumab plus bevacizumab in unresectable hepatocellular carcinoma. N Engl J Med 2020; 382:1894–1905. [PubMed: 32402160]

7. Greten TF, Mauda-Havakuk M, Heinrich B, Korangy F, Wood BJ. Combined locoregional-immunotherapy for liver cancer. J Hepatol 2019;70:999–1007. [PubMed: 30738077]

8. Mehta A, Oklu R, Sheth RA. Thermal ablative therapies and immune checkpoint modulation: can locoregional approaches effect a systemic response? Gastroenterol Res Pract 2016; 2016:9251375. [PubMed: 27051417]

9. Bogdanos DP, Gao B, Gershwin ME. Liver immunology. Compr Physiol 2013; 3:567–598. [PubMed: 23720323]

10. Adamus T, Kortylewski M. The revival of CpG oligonucleotide-based cancer immunotherapies. Contemp Oncol (Pozn) 2018; 22:56–60. [PubMed: 29628795]

11. Thomson AW, Knolle PA. Antigen-presenting cell function in the tolerogenic liver environment. Nat Rev Immunol 2010; 10:753–766. [PubMed: 20972472]

12. Karapetyan L, Luke JJ, Davar D. Toll-like receptor 9 agonists in cancer. Onco Targets Ther 2020; 13:10039–10060. [PubMed: 33116588]

13. Nierkens S, den Brok MH, Sutmuller RP, et al. In vivo colocalization of antigen and CpG [corrected] within dendritic cells is associated with the efficacy of cancer immunotherapy. Cancer Res 2008; 68:5390–5396. [PubMed: 18593941]

14. Ribas A, Medina T, Kummar S, et al. SD-101 in combination with pembrolizumab in advanced melanoma: results of a phase Ib, multicenter study. Cancer Discov 2018; 8:1250–1257. [PubMed: 30154193]

15. Wang K, Wang C, Jiang H, et al. Combination of ablation and immunotherapy for hepatocellular carcinoma: where we are and where to go. Front Immunol 2021; 12:792781. [PubMed: 34975896]

16. Zender L, Xue W, Cordon-Cardo C, et al. Generation and analysis of genetically defined liver carcinomas derived from bipotential liver progenitors. Cold Spring Harb Symp Quant Biol 2005; 70:251–261. [PubMed: 16869761]

17. Curiel TJ. Regulatory T cells and treatment of cancer. Curr Opin Immunol 2008; 20:241–246. [PubMed: 18508251]

18. Topham DJ, Reilly EC. Tissue-resident memory CD8+ T cells: from phenotype to function. Front Immunol 2018; 9:515. [PubMed: 29632527]

19. Susek KH, Karvouni M, Alici E, Lundqvist A. The role of CXC chemokine receptors 1-4 on immune cells in the tumor microenvironment. Front Immunol 2018; 9:2159. [PubMed: 30319622]

20. Huo Y, Chen WS, Lee J, Feng GS, Newton IG. Stress conditions induced by locoregional therapies stimulate enrichment and proliferation of liver cancer stem cells. J Vasc Interv Radiol 2019; 30:2016–2025. [PubMed: 31208945]

21. Gocher AM, Workman CJ, Vignali DA. Interferon-γ: teammate or opponent in the tumour microenvironment? Nat Rev Immunol 2022; 22:158–172. [PubMed: 34155388]

22. Zheng H, Ban Y, Wei F, Ma X. Regulation of interleukin-12 production in antigen-presenting cells. Adv Exp Med Biol 2016; 941:117–138. [PubMed: 27734411]

23. Joss A, Akdis M, Faith A, Blaser K, Akdis CA. IL-10 directly acts on T cells by specifically altering the CD28 co-stimulation pathway. Eur J Immunol 2000; 30:1683–1690. [PubMed: 10898505]

24. Tiemessen MM, Kunzmann S, Schmidt-Weber CB, et al. Transforming growth factor-β inhibits human antigen-specific CD4+ T cell proliferation without modulating the cytokine response. Int Immunol 2003; 15:1495–1504. [PubMed: 14645158]

25. Okada Y, Wang T, Kasai K, Suzuki K, Takikawa Y. Regulation of transforming growth factor is involved in the efficacy of combined 5-fluorouracil and interferon alpha-2b therapy of advanced hepatocellular carcinoma. Cell Death Discov 2018; 4:42.

26. Zoglmeier C, Bauer H, Nörenberg D, et al. CpG blocks immunosuppression by myeloid-derived suppressor cells in tumor-bearing mice. Clin Cancer Res 2011; 17:1765–1775. [PubMed: 21233400]

27. Yu GT, Bu LL, Huang CF, et al. PD-1 blockade attenuates immunosuppressive myeloid cells due to inhibition of CD47/SIRPα axis in HPV negative head and neck squamous cell carcinoma. Oncotarget 2015; 6:42067–42080. [PubMed: 26573233]

28. Bent R, Moll L, Grabbe S, Bros M. Interleukin-1 beta—a friend or foe in malignancies? Int J Mol Sci 2018; 19:2155. [PubMed: 30042333]

29. Wherry EJ. T cell exhaustion. Nat Immunol 2011; 12:492–499. [PubMed: 21739672]

30. Pfister D, Núñez NG, Pinyol R, et al. NASH limits anti-tumour surveillance in immunotherapy-treated HCC. Nature 2021; 592:450–456. [PubMed: 33762733]

31. Schumacher TN, Schreiber RD. Neoantigens in cancer immunotherapy. Science 2015; 348:69–74. [PubMed: 25838375]

RESEARCH HIGHLIGHTS

- Cotreatment with a programmed cell death 1 inhibitor and CpG or CpG alone at the time of incomplete cryoablation prolonged the time to endpoints compared with cryoablation alone (log-rank hazard ratio, 0.27; $P < .001$ and log-rank hazard ratio, 0.42; $P = .031$ respectively).
- A programmed cell death 1 inhibitor with CpG or CpG alone at the time of incomplete cryoablation also decreased the growth rate of simulated metastatic liver tumors compared with cryoablation alone (2.8-fold, $P = .007$ and 1.9-fold, $P = .047$, respectively).
- Flow cytometry and histology demonstrated CD8+ and NK+ cell infiltration of treated and metastatic tumors among CpG-treated mice, and serum cytokine changes were consistent with antitumoral immunity.

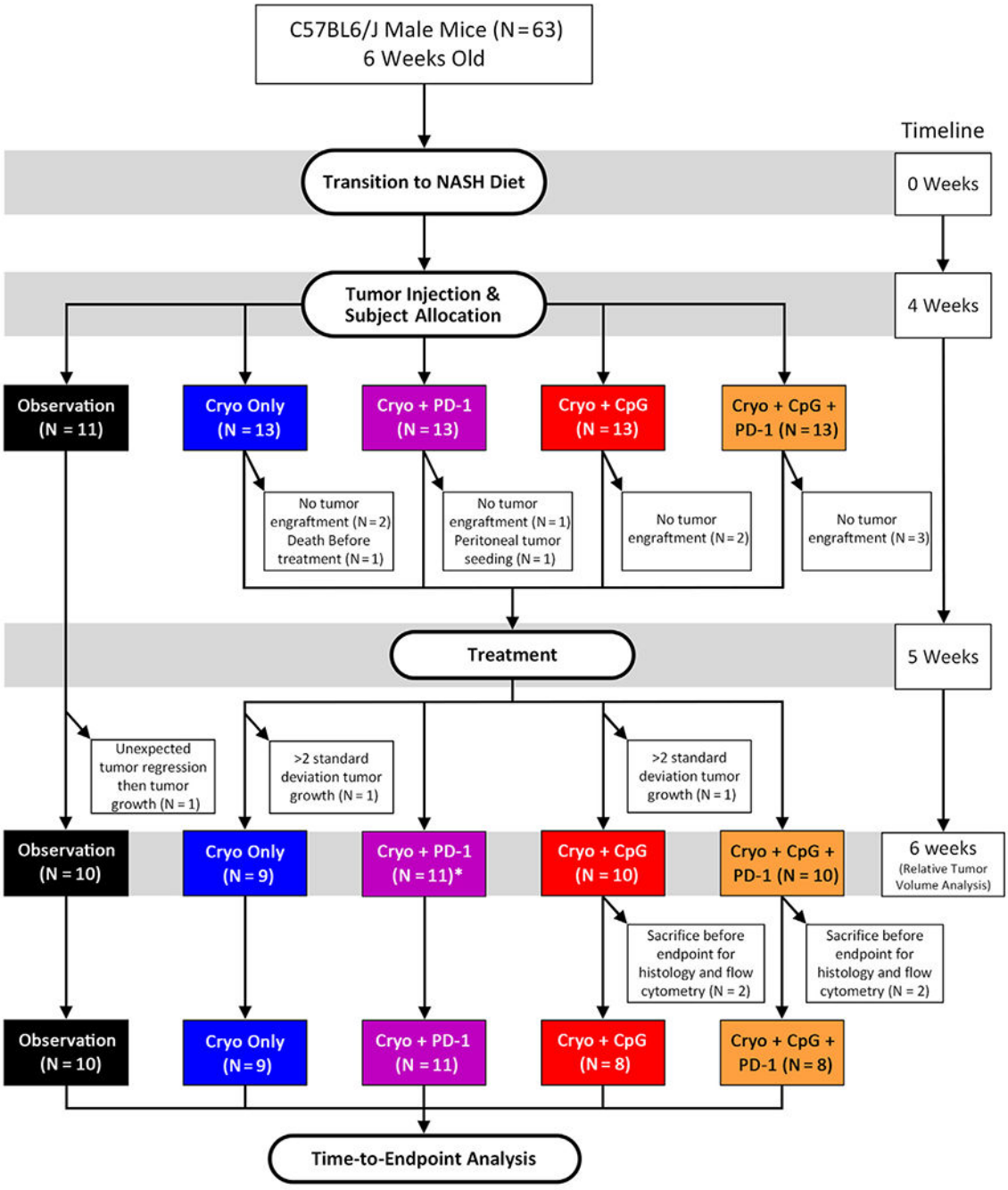

Figure 1.

Flow diagram of subject exclusion for time-to-endpoint analysis. *A cryoablation + programmed cell death 1 (n = 1) mouse died before the 6-week time point and was included in the time-to-endpoint data (n = 11 subjects) but not the relative tumor volume data (n = 10 subjects). Cryo = cryoablation; NASH = nonalcoholic steatohepatitis; PD-1 = programmed cell death 1.

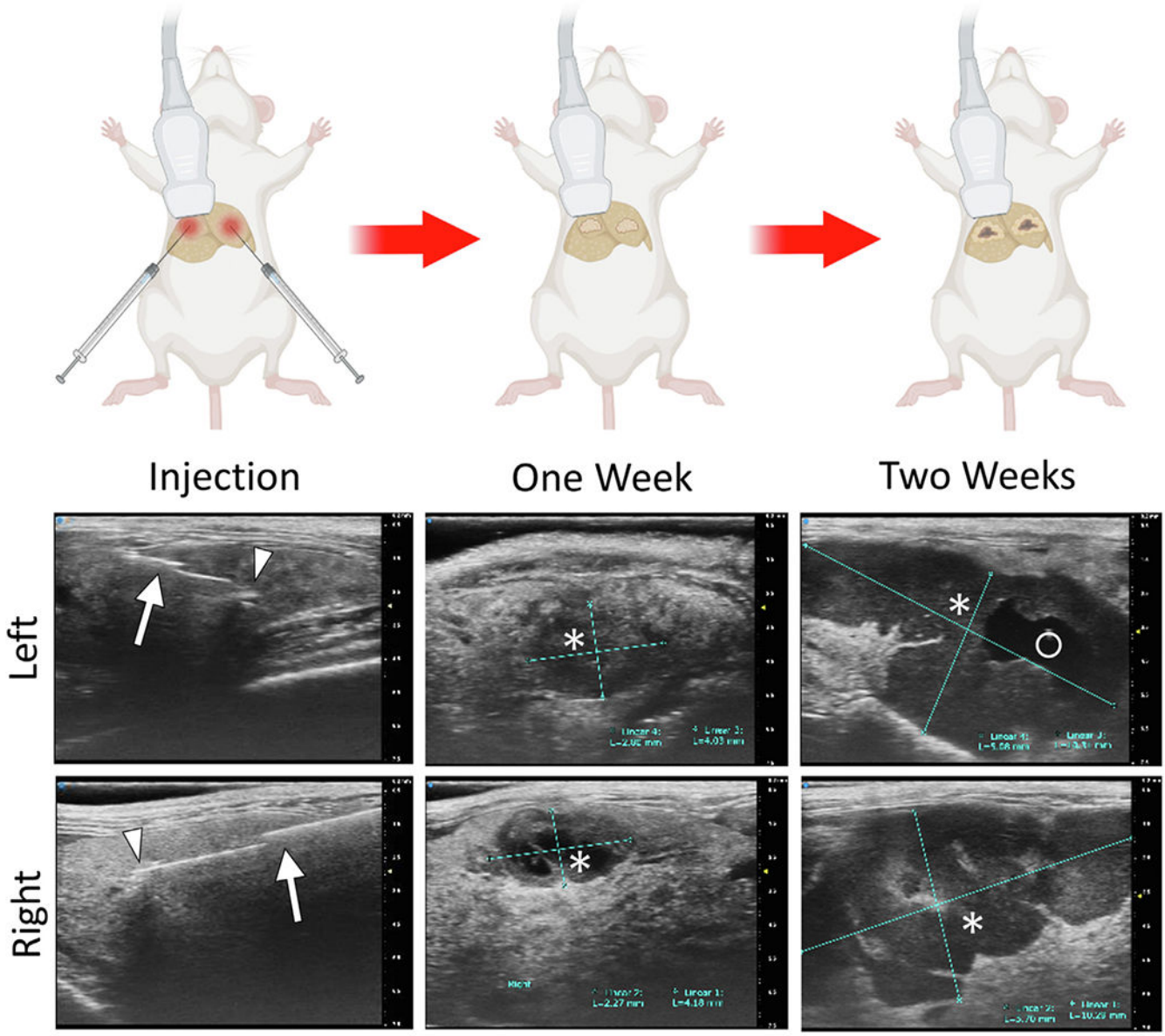

Figure 2.

Tumor injection and engraftment. Tumors were injected using a coaxial technique into the left and right hepatic lobes. Arrows denote the outer introducer needle. Arrowheads denote the inner injection needle. The tumors grew rapidly (*), at times demonstrating cystic necrosis (O).

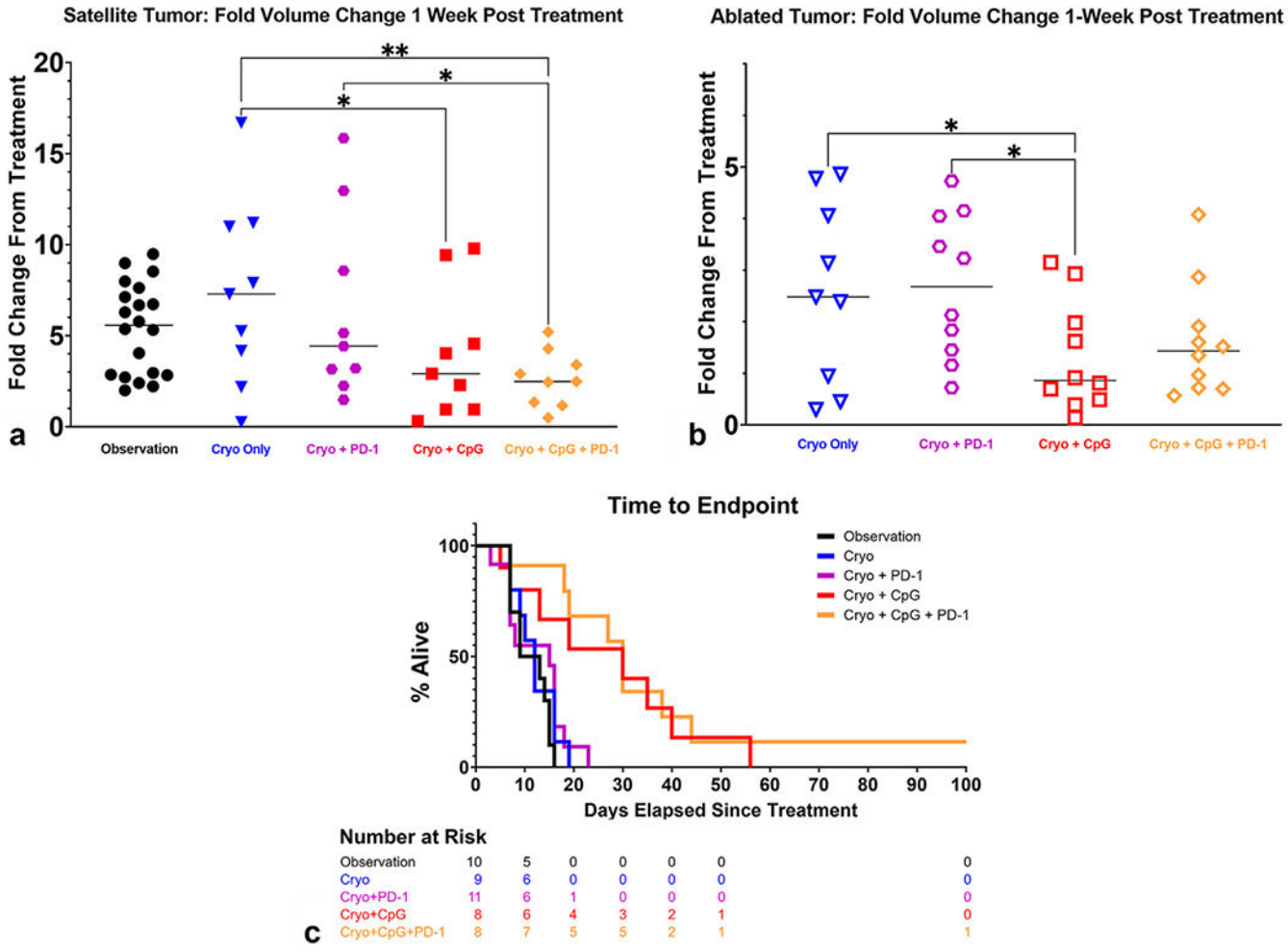

Figure 3.

Relative tumor volume change at 1 week after treatment. **(a)** Nonablated satellite and **(b)** ablated tumor volumes from untreated mice and mice that underwent cryoablation (cryo), cryo + intratumoral CpG injection, cryo + programmed cell death 1 (PD-1) injection, or cryo + CpG + PD-1 treatment were calculated at 1 week after treatment, and fold change in the pretreatment tumor volume was determined. Treatment with cryo + CpG was associated with a statistically significant tumor growth retarding effect in both ablated and nonablated tumors compared with cryo alone (*$P < .05$, **$P < .01$). **(c)** Single tumor treatment with cryo CpG or cryo + CpG + PD-1 delayed the time to endpoint, with log-rank hazard ratios of 0.42 ($P = .031$) and 0.27 ($P < .001$), respectively, compared with cryo (C).

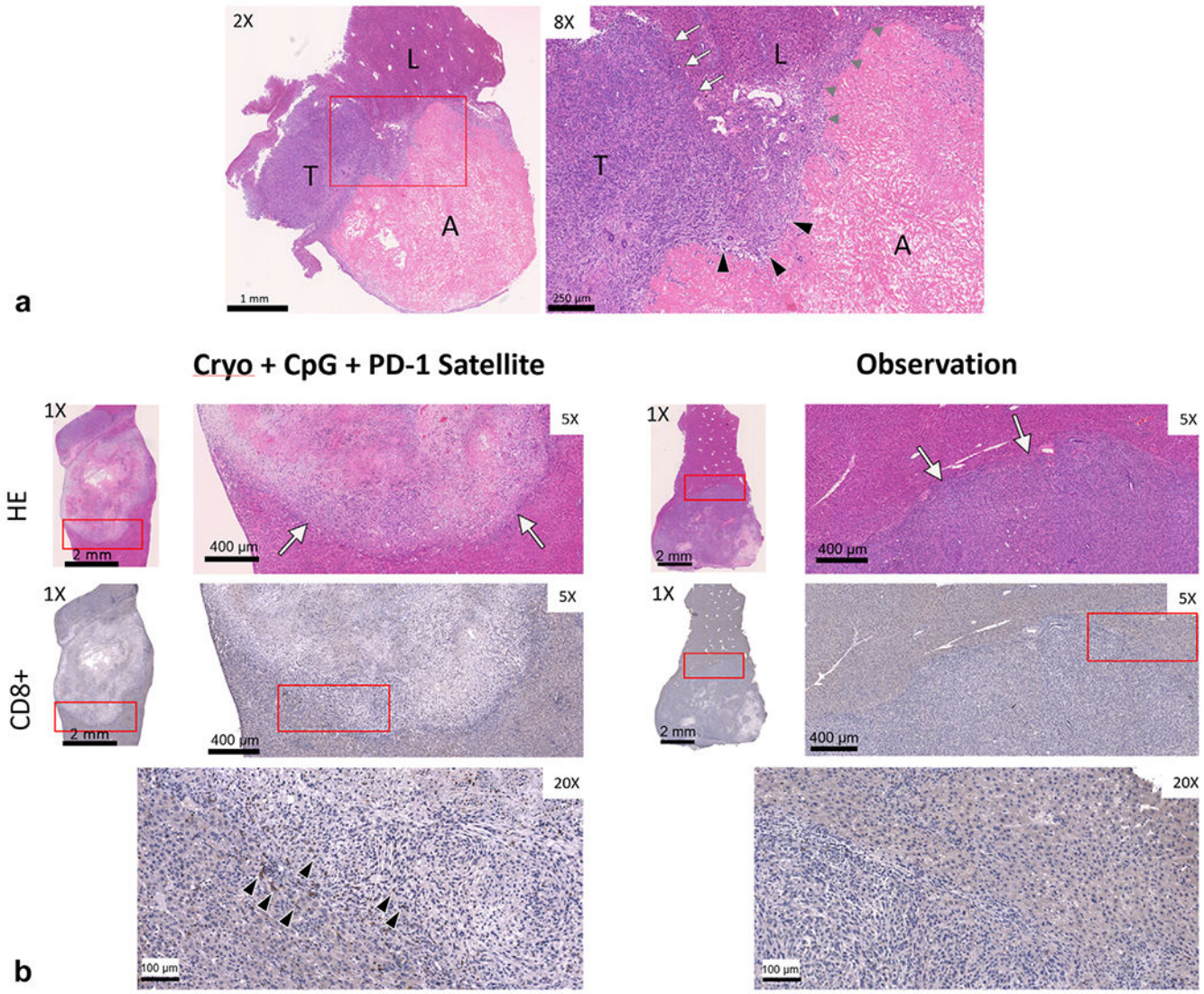

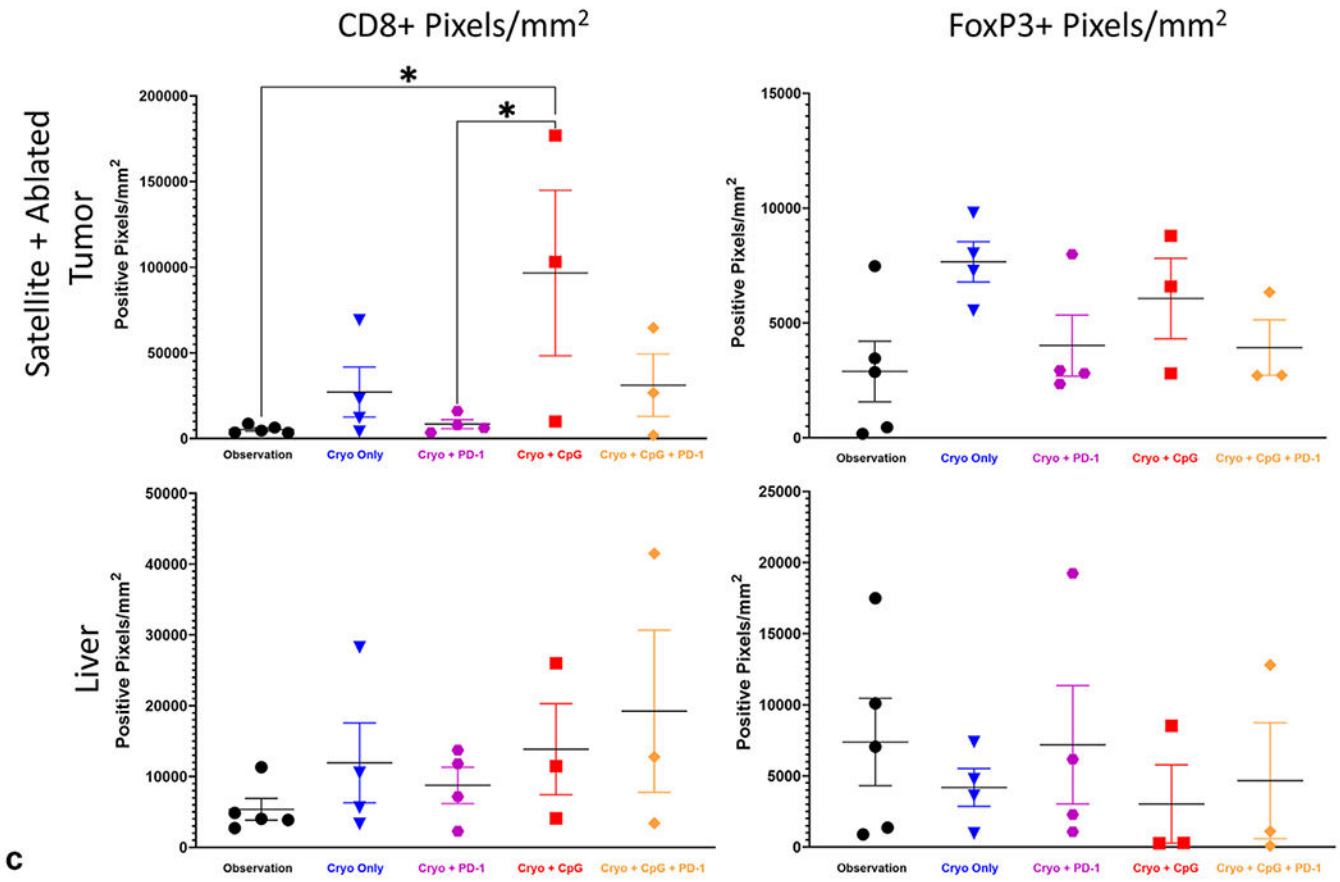

Figure 4.

Histology. **(a)** Hematoxylin and eosin staining of an incompletely ablated intrahepatic tumor from a mouse treated with cryoablation (cryo) + CpG + programmed cell death 1 (PD-1). At 2× (left) and 8× (right) magnifications of normal hepatic parenchyma, tumor tissue characterized by small cells with large nuclei and a large nuclear-to-cytoplasmic ratio, and the highly eosinophilic and acellular ablation zone. A few small infiltrating cells are seen, many of which are lymphocytes. The liver-tumor interface (arrows), ablation-tumor (black arrowheads), and ablation-liver (gray arrowheads) interfaces are well demarcated at 8× magnification. **(b)** Qualitatively, cytotoxic CD8+ T cells accumulated at the tumor periphery in CpG-treated mice at 1 week after treatment. The liver-tumor interface is delineated by arrows in the hematoxylin and eosin staining image. Arrowheads show cytotoxic CD8+ T cells accumulated at the liver-tumor interface of the cryo + CpG + PD-1–treated subject. **(c)** Immunohistochemistry directed at CD8 and FOXP3 of normal liver and pooled viable ablated and nonablated tumor tissue from animals sacrificed at 1 week after treatment. Positive pixels were detected by software and normalized to the area of analyzed tissue to create positive pixel density (*$P < .05$). A = ablation zone; HE = hematoxylin and eosin; L = normal hepatic parenchyma; T = tumor tissue.

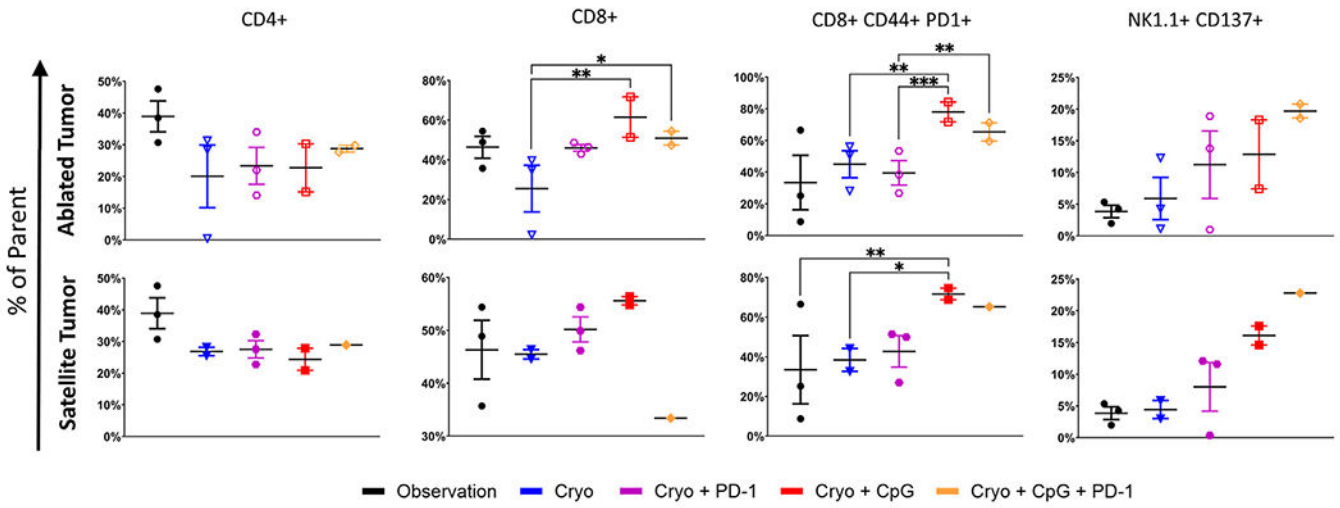

Figure 5.

Multiparametric flow cytometric analysis of ablated and nonablated (satellite) tumor tissue collected at 1 week after treatment. CD4+ and CD8+ were expressed as the percentage of CD3+ cells, NK+ CD137+ as the percentage of NK+ cells, and CD44+ PD-1+ as the percentage of CD8+ cells. CpG treatment was associated with cytotoxic CD8+ T-cell enrichment in ablated tumor tissue. CpG injection was strongly associated with increased programmed cell death 1 expression by activated cytotoxic T cells (CD44+ CD8+) in all tested tissue types (*$P < .05$, **$P < .01$, ***$P < .001$). Cryo = cryoablation; PD-1 = programmed cell death 1.

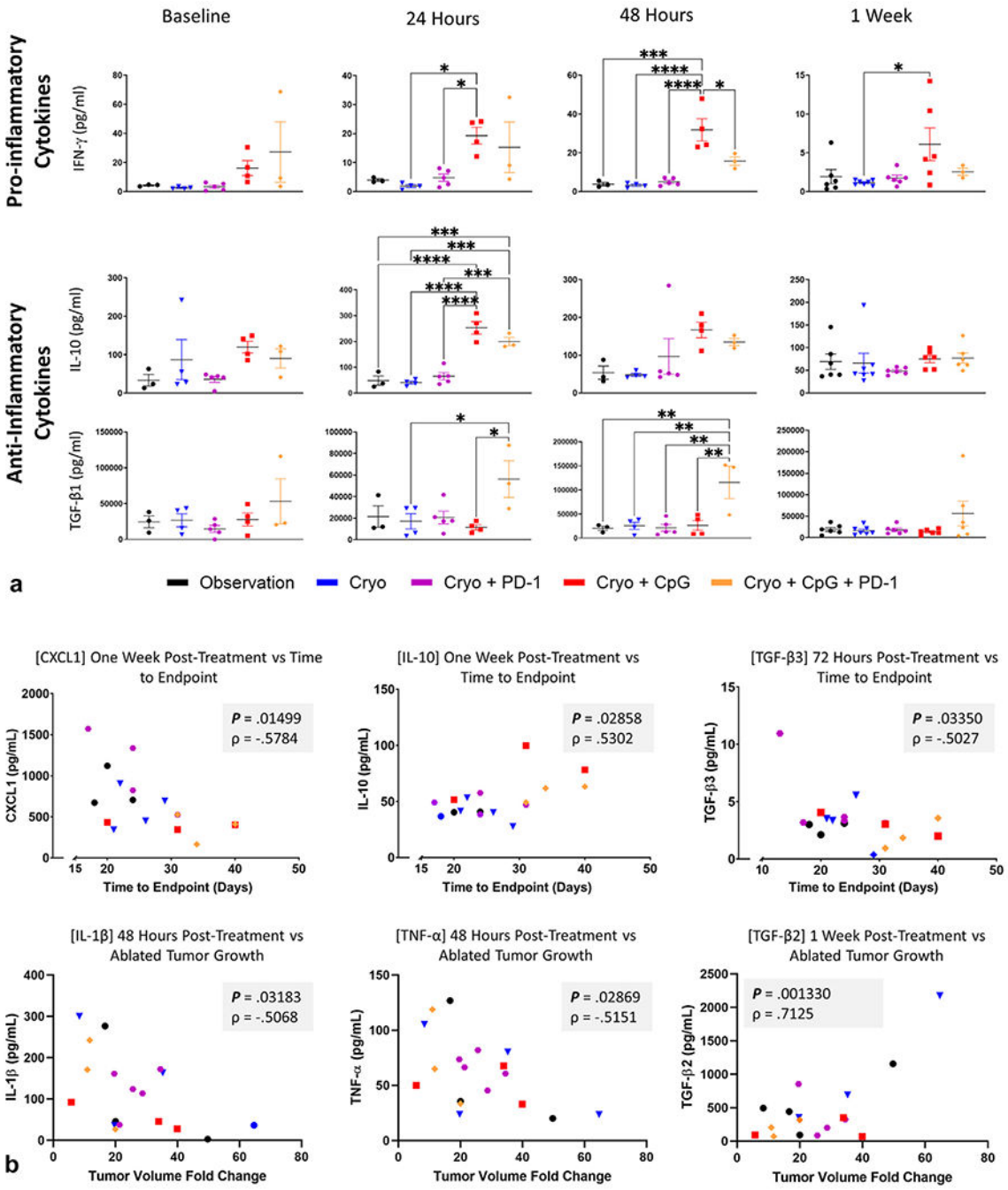

Figure 6.

Proinflammatory and anti-inflammatory serum cytokines at 1 week after treatment. **(a)** The serum levels of the proinflammatory cytokine interferon-γ and anti-inflammatory cytokines tumor growth factor-β1 and interleukin-10 were quantitated at baseline, 24 hours, 48 hours, and 1 week following treatment. **(b)** A linear correlation model (Pearson) was applied to cytokine concentrations at baseline; 24, 48, and 72 hours; and 1 and 2 weeks after treatment and compared with overall survival (top) and fold change of ablated tumor volume (bottom) at 1 week compared with that at the baseline. Statistically significant ($P < .05$) results

are shown. Cryo = cryoablation; IFN-γ = interferon-γ; PD-1 = programmed cell death 1; TGF-β1 = transforming growth factor-β1.

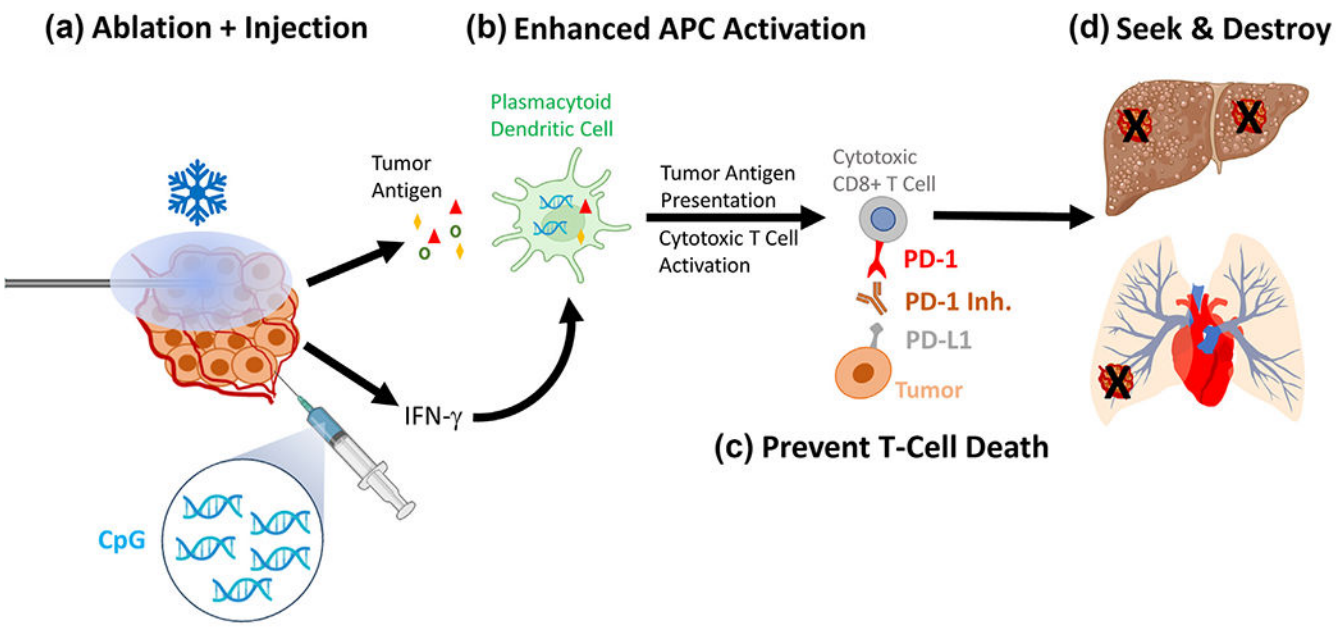

Figure 7.

Proposed mechanism for cytotoxic T-cell (CTL) antitumoral immunity. **(a)** Tumors were cryoablated and coinjected with CpG, thereby releasing tumor antigens and stimulating proinflammatory cytokines (eg, interferon-γ). **(b)** Tumor antigens are taken up by circulating plasmacytoid dendritic cells, which are stimulated by CpG and proinflammatory cytokines to crosspresent the tumor antigens and activate CTLs. **(c)** Programmed cell death 1 inhibition at the time of tumor antigen cross-presentation prevents programmed death ligand 1–mediated CTL anergy and clonal deletion. **(d)** Tumor antigen crosspresentation and activation leads to CTL-mediated antitumoral immunity. APC = antigen-presenting cell; IFN-γ = interferon-γ; Inh. = inhibitor; PD-1 = programmed cell death 1; PD-L1 = programmed death ligand 1